

Histone deacetylase 9 activates IKK to regulate atherosclerotic plaque vulnerability

Short Title: *Asare et al.; Targeting HDAC9 confers plaque stability*

Yaw Asare, PhD¹; Thomas A. Campbell-James¹; Yury Bokov¹; Lydia Luya Yu¹; Matthias Prestel, PhD¹; Omar El Bounkari, PhD¹; Stefan Roth, PhD¹; Remco T.A. Mogens, PhD^{2,3}; Tobias Straub, PhD⁴; Kyra Thomas¹, Guangyao Yan, MSc¹; Melanie Schneider¹, Natalie Ziesch¹, Steffen Tiedt, MD, PhD¹; Carlos Silvestre-Roig, PhD²; Quinte Braster, MSc²; Yishu Huang, MSc¹; Manuela Schneider, DVM¹; Rainer Malik, PhD¹; Christof Haffner, PhD¹; Arthur Liesz, MD^{1, 5}; Oliver Soehnlein, MD, PhD^{2, 6, 7}; Jürgen Bernhagen, PhD^{1, 5, 6}; Martin Dichgans, MD^{1, 5}

¹Institute for Stroke and Dementia Research (ISD), University Hospital, Ludwig-Maximilians-University LMU, Munich, Germany; ²Institute for Cardiovascular Prevention, Ludwig-Maximilians-University Munich LMU, Germany; ³Department of Biomedical Engineering, Cardiovascular Research Institute Maastricht, Maastricht University, the Netherlands; ⁴BMC, Core Facility Bioinformatics Munich, Germany; ⁵Munich Cluster for Systems Neurology (Synergy), Munich, Germany; ⁶German Center for Cardiovascular Research (DZHK), Partner Site Munich Heart Alliance, Munich, Germany; ⁷Department of Physiology and Pharmacology, Karolinska Institute, Stockholm, Sweden.

Address for Correspondence:

Prof. Dr. Martin Dichgans
Institute for Stroke and Dementia Research
Klinikum der Universität München
Feodor-Lynen-Straße 17, D-81377 München
Telefon: +49 (0)89 4400 - 46019
Fax: +49 (0)89 4400 - 46010
E-Mail: martin.dichgans@med.uni-muenchen.de
Internet: <https://www.isd-research.de/isd-research>

Total word count: 7,963

Subject codes: Atherosclerosis, Inflammation, Mechanisms, Vascular Biology

Abstract

Rationale: Arterial inflammation manifested as atherosclerosis is the leading cause of mortality worldwide. Genome-wide association studies have identified a prominent role of histone deacetylase 9 (HDAC9) in atherosclerosis and its clinical complications including stroke and myocardial infarction.

Objective: To determine the mechanisms linking HDAC9 to these vascular pathologies and explore its therapeutic potential for atheroprotection.

Methods and Results: We studied the effects of *Hdac9* on features of plaque vulnerability using bone marrow reconstitution experiments and pharmacological targeting with a small molecule inhibitor in hyperlipidemic mice. We further employed two-photon and intravital microscopy to study endothelial activation and leukocyte-endothelial interactions. We show that hematopoietic *Hdac9* deficiency reduces lesional macrophage content whilst increasing fibrous cap thickness thus conferring plaque stability. We demonstrate that HDAC9 binds to IKK α and β resulting in their deacetylation and subsequent activation, which drives inflammatory responses in both macrophages and endothelial cells. Pharmacological inhibition of HDAC9 with the class IIa HDAC inhibitor TMP195 attenuates lesion formation by reducing endothelial activation and leukocyte recruitment along with limiting pro-inflammatory responses in macrophages. Transcriptional profiling using RNA-Seq revealed that TMP195 downregulates key inflammatory pathways consistent with inhibitory effects on IKK β . TMP195 mitigates the progression of established lesions and inhibits the infiltration of inflammatory cells. Moreover, TMP195 diminishes features of plaque vulnerability and thereby enhances plaque stability in advanced lesions. *Ex vivo* treatment of monocytes from patients with established atherosclerosis reduced the production of inflammatory cytokines including IL-1 β and IL-6.

Conclusion: Our findings identify HDAC9 as a regulator of atherosclerotic plaque stability and IKK activation thus providing a mechanistic explanation for the prominence of HDAC9 as a vascular risk locus in genome-wide association studies. Its therapeutic inhibition may provide a potent lever to alleviate vascular inflammation.

Key Words: HDAC9, IKK, atherosclerosis, inflammation, plaque vulnerability

Nonstandard Abbreviations and Acronyms:

GWAS	Genome-wide association studies
HDAC9	Histone deacetylase 9
NF- κ B	Nuclear factor-kappa-light-chain-enhancer of activated B-cells
IKK	Inhibitory Kappa B Kinase
GSK3 β	Glycogen synthase kinase 3 beta
RSK1	Ribosomal s6 kinase
Apoe	Apolipoprotein e
HUVECs	Human umbilical vein endothelial cells
I κ B- α	Inhibitor of kappa B
BMDMs	Bone marrow-derived macrophages

Introduction

Arterial inflammation manifested as atherosclerosis is the main underlying pathology of cardiovascular disease including stroke and myocardial infarction ¹. As a chronic inflammatory condition, atherosclerosis is orchestrated by numerous mediators of innate and adaptive immune responses ^{2, 3}. Critical steps in atherogenesis include activation of the vascular endothelium and subsequent recruitment of immune cells. Inflammatory myeloid cells dominate both disease initiation and progression, while expansion of the necrotic core and fibrous cap thinning dictate plaque stability ^{4, 5}.

Histone deacetylases (HDACs) are signal-responsive regulators of gene expression with established roles in innate and adaptive immune pathways ⁶⁻⁸. Class IIa HDACs (HDAC4, 5, 7, and 9) shuttle between the cytoplasm and nucleus and control expression of key mediators of vascular inflammation ⁶. HDAC9 stands out as an important regulator of cell differentiation ⁹, proliferation ¹⁰, angiogenesis ¹¹, glucose, and lipid metabolism ^{12, 13}. We and others previously demonstrated a prominence of HDAC9 in human atherosclerosis by genome-wide association studies (GWAS) in stroke ^{14, 15}, coronary artery disease and myocardial infarction ¹⁶, atherosclerotic aortic calcification ¹⁷, and peripheral artery disease ¹⁸. In spite of these striking associations, the mechanisms linking HDAC9 to vascular inflammation and the ensuing therapeutic potential remain poorly defined.

Here, we set out to address this gap by combining experiments in genetic mouse models with pharmacological targeting. We show that HDAC9 regulates features of atherosclerotic plaque vulnerability and demonstrate binding of HDAC9 to the NF- κ B activating kinases IKK α and IKK β resulting in their deacetylation and subsequent activation. Moreover, pharmacological inhibition

of these HDAC9-dependent mechanisms stabilized atherosclerotic lesions in mice and limited the activation of monocytes obtained from patients with established atherosclerosis.

Methods

Mouse model of atherosclerosis

Sample size for mouse experiments was determined by SigmaPlot 12.5 with 80% statistical power and an α error of 0.05 on the basis of previous experiments^{19,20}. Mice were randomly assigned to groups and data collection and analysis were performed blinded. Data were excluded for mice with broken aortic root valves after sectioning of the heart or died during treatment. *Hdac9*^{-/-}*ApoE*^{-/-} mice were generated as previously described²¹. Mice had ad libitum access to food and water and were housed in a specific pathogen-free animal facility under a 12 h light-dark cycle. All mice used were males and experiments were started when mice were 6-8 weeks old. For the treatment approach, *ApoE*^{-/-} mice (B6.129P2-*ApoE*/J; Charles River Laboratories) were fed a Western-type diet containing 21% fat (TD88137, Ssniff) for 4 weeks to induce early atherosclerosis and in parallel received daily intraperitoneal (i.p.) injections of TMP195 (50 mg/kg, Axon Medchem) or DMSO (vehicle) control solvent²². To study the effects of TMP195 on established lesions, *ApoE*^{-/-} mice were fed a Western-type diet for 8 weeks and starting in the 5th week, received daily i.p. injections of TMP195 (50 mg/kg) or vehicle. Features of plaque vulnerability, determined as macrophage area x necrotic core area / smooth muscle cell area x collagen area²⁰, were examined in *ApoE*^{-/-} mice that were fed Western-type diet for 11 weeks and starting in the 8th week, were treated with TMP195 (50 mg/kg) or vehicle. Atherosclerotic lesions were quantified on serial sections by histology and immunofluorescence. Cholesterol and triglyceride levels in plasma were

quantified using enzymatic assays (Cayman) according to the manufacturer's protocol. All animal experiments were approved by the local ethics committee.

Bone marrow transplantation

Recipient *ApoE*^{-/-} mice were exposed to a lethal dose of whole-body irradiation (2x 6.5Gy) a day before bone marrow transplantation and transplanted with bone marrow from *Hdac9*^{-/-}*ApoE*^{-/-} and control *Hdac9*^{+/+}*ApoE*^{-/-} donors. Irradiated mice were allowed to recuperate for 4 weeks on antibiotics before receiving Western-type diet for 11 weeks.

Tissue Harvesting

Mice were anesthetized using ketamine-xylazine or medetomidine-midazolam-fentanyl. Blood was obtained via cardiac puncture and the arterial tree was perfused through the left ventricle with 0.9% sterile NaCl. Hearts were either fixed in 4% paraformaldehyde (PFA) or directly embedded in Tissue-Tek OCT for sectioning and quantification of atherosclerotic lesion sizes. For protein analysis via western blot, the whole aorta was dissected, flash-frozen and lysed in RIPA buffer containing complete EDTA-free phosphatase and protease inhibitors (Roche) using the Ika T8 Ultra Turrax Tissue Homogenizer. Where indicated, carotid arteries were flash-frozen for RNA isolation and real time PCR analysis.

Immunohistochemistry

The extent of atherosclerosis was assessed in the aortic root by staining lipid depositions with Oil-red O. Hearts were embedded in Tissue-Tek for cryosectioning. Atherosclerotic lesions were quantified in 5 µm transverse serial sections and averages calculated from 3-5 sections. Masson

trichrome staining was performed on both aortic root and paraffin-embedded aortic arch sections to analyze lesion size, collagen content, fibrous cap thickness, and necrotic core formation. Macrophages and smooth muscle cells (SMCs) were visualized by immunofluorescent staining for Cd68 (Sigma) or Mac2 (Cedarlane) followed by Alexa 488-conjugated affinity purified antibody (Jackson ImmunoResearch) and Sma-cy3 (Sigma), respectively. Nuclei were counterstained by 4', 6-diamidino-2-phenylindol (DAPI). All images were recorded with a Leica DMLB fluorescence microscope and CCD camera, and quantification of lesion size and composition was performed using Image J analysis software.

Intravital microscopy

Cx3cr1^{gfp/wt}ApoE^{-/-} mice were fed a Western-type diet for 4 weeks, and in parallel received TMP195 (50 mg/kg) or vehicle. Following cannulation of the right jugular vein with a catheter, antibodies against Ly6G (1A8, Biolegend) and CD11b (M1/70, eBioscience) were administered and allowed to circulate for 10 min to label myeloid cell subsets. Subsequently, the left carotid artery was surgically exposed and intravital microscopy was performed using an Olympus BX51 microscope equipped with a Hamamatsu 9100-02 EMCCD camera and a 10x saline-immersion objective. Image acquisition and analysis was performed with the Olympus excellence software.

Two-photon imaging of whole-mount tissue

Cx3cr1^{gfp/wt}ApoE^{-/-} mice were fed a Western-type diet for 4 weeks, and in parallel received TMP195 (50 mg/kg) or vehicle. Fresh carotid arteries were explanted and mounted on glass micropipettes at a pressure of 80 mmHg. CD31 and VCAM-1 expression were quantified using CD31 (#48031182, eBioscience) and VCAM-1 (#105724, Biolegend) antibodies. The samples

were imaged using a Leica SP5IIMP two-photon laser scanning microscope with a pre-chirped and pulsed Ti:Sapphire Laser (Spectra Physics MaiTai Deepsee) tuned at 790nm and a 20×NA1.00 (Leica) water dipping objective. Image acquisition and processing was performed using LasX software (Leica).

Patient population and blood sampling

Patients with acute ischemic stroke were recruited in 2017 through the stroke service, Klinikum der Universität München (KUM), a tertiary level hospital at Ludwig-Maximilians-Universität (LMU), Munich, Germany. Patients were selected based on the presence of carotid atherosclerosis (carotid artery plaques or carotid artery stenosis) documented by carotid ultrasound. Whole blood was drawn into EDTA-plasma containers (Sarstedt) using a tourniquet and 21-gauge needles. The study was approved by the local ethics committee and was conducted in accordance with the Declaration of Helsinki as well as institutional guidelines. Written and informed consent was obtained from all subjects.

Isolation of human monocytes

Human Peripheral Blood Mononuclear Cells (PBMCs) were isolated from whole blood by Ficoll-Paque (GE Healthcare) density gradient centrifugation and were enriched for monocytes with the Monocyte Isolation Kit II (Miltenyi Biotec) according to manufacturer's recommendation. A cocktail of biotin-conjugated antibodies was used to label non-monocytes. Depletion of these labeled cells resulted in enriched monocytes.

Primary cell culture, transfection and gene silencing

Human Umbilical Vein Endothelial Cells (HUVECs) were purchased from PromoCell, plated on cell culture dishes coated with collagen (Biochrom AG), cultured in endothelial cell growth medium (PromoCell) according to manufacturer's recommendations and used between passages 5 and 8. Transfection of HUVECs with predesigned ON-TARGETplus SMARTpool human *HDAC9* siRNA or Non-targeting control (Dharmacon) was conducted by electroporation using the HUVEC Nucleofector Kit (Lonza) following the manufacturer's instructions. Where indicated, plasmid DNA was co-transfected. Cells recuperated for 48 h or 72 h before entering the experiment. HUVEC were stimulated with 20 ng/ml human TNF- α (PeproTech) at different time intervals.

Generation of bone marrow-derived macrophages

Bone marrow-derived macrophages (BMDMs) were generated as established by flushing the bone marrow from femurs and tibiae with ice-cold PBS, resuspending in PBS by repeated pipetting and filtering through a 40 μ m cell strainer (BD Biosciences). After centrifugation of the cell suspension at 500 g for 10 min, the pellet was resuspended in culture medium (RPMI 1640 containing 10% FCS, 15% L929-cell-conditioned medium (LCM) and 100 μ l/ml gentamycin) and plated on 15 cm untreated culture plates (Greiner). 15 % fresh L929-conditioned medium (LCM) was added again on day 1 and 2 of culturing. For stimulation experiments, differentiated macrophages were harvested by gentle scraping, transferred onto untreated 6-well or 12-well plates (Greiner) on Day 7 of culturing and left in LCM-free medium for 24 hours, allowing cells to adhere. Cells were then stimulated in FCS-free medium with either 50 ng/ml mouse recombinant Tnf- α at different time intervals or left untreated.

Flow cytometry

Aorta and EDTA-buffered blood samples were harvested and a single-cell suspension was prepared and filtered over a 70 μm cell strainer (Greiner). Cells were treated with erythrocyte lysis buffer (0.155 M NH_4Cl , 10 mM NaHCO_3). All cell suspensions were carefully washed and stained with FACS staining buffer and combinations of antibodies against Cd45, Cd11b, Cd3, B220, Ly6G (eBioscience), and Ly6C (Miltenyi Biotec). Flow cytometry analysis was performed using FACSVerse and FACSuite software (BD Biosciences) after appropriate fluorescence compensation, and leukocyte subsets were gated using FlowJo software (Treestar). B cells were identified as $\text{Cd45}^+\text{B220}^+$; T cells as $\text{Cd45}^+\text{Cd3}^+$; neutrophils as $\text{Cd45}^+\text{CD11b}^+\text{Ly6G}^+$; monocytes as $\text{Cd45}^+\text{Cd11b}^+\text{Ly6C}^+$.

RNAseq analysis

BMDMs were isolated from *ApoE*^{-/-} mice as established and briefly described above. Cells were pretreated with either TMP195 (5 μM) or TPCA-1 (500 nM) for 1 h prior to stimulation with $\text{TNF-}\alpha$ (50 ng/ml) for 24 h. Total RNA was isolated using Trizol (Invitrogen) and RNA library prepared according to Illumina RNA Seq library kit instructions. Quality control and quantification of RNA and library were performed using an Agilent 2100 Bioanalyzer and a Kapa Library Quantification Kit (Kapa Biosystems), according to the manufacturer's protocol. cDNA fragments were amplified with Illumina's cBot. Libraries were loaded at a concentration of 10 pM onto flow cells and sequenced on an Illumina HiSeq 1500 platform.

For sequence analysis of RNA reads, 50 nt single-end reads were mapped to the GRCm38 reference genome using STAR software version 2.6.1d. TPM expression values based on ENSEMBL annotation version GRCm38.95 were calculated with RSEM (1.3.0). We used the

DESeq2 Bioconductor R package to identify differentially expressed genes at a false discovery rate (FDR) of 10%. Gene ontology enrichment was determined using 'topGO' (2.36.0), Gene set enrichment analysis (GSEA) was performed using the 'fgsea' package (1.10.0).

Quantitative real-time PCR

RNA was isolated using the RNeasy Mini Kit (Qiagen) and reverse-transcribed using oligodT primers (Metabion). RT-PCR analysis was performed using Brilliant II SYBR Green QPCR Master Mix (Agilent Technologies) in a Light cycler 480 (Roche Diagnostics). *GAPDH*, *HPRT1* or *18S* were used as housekeeping genes, as appropriate. Measurements were performed in triplicates. The $2^{-\Delta\Delta Ct}$ method was used to calculate relative expression changes.

ELISA

Cytokine levels in mouse plasma were measured using a commercially available kit for Ccl2 (Invitrogen). For cytokine secretion, BMDMs were stimulated with 50 ng/ml mouse Tnf- α (Peprotech) for the indicated times. Levels of Cxcl1, Il-1 β , Il-6, Tnf- α and Ccl2 were assayed in the supernatant using commercially available ELISA kits (R&D systems). Likewise, the secretion of human TNF- α , CCL2, IL-1 β and IL-6 were quantified using commercially available ELISA kits (Invitrogen and R&D systems).

Cell lysis, co-immunoprecipitation and Western blot analysis

For total cell lysates, cells were washed with cold PBS and lysed either directly with 1x NuPAGE-LDS-sample buffer (Invitrogen) containing 1 mmol/l DTT (Sigma Aldrich) or with 1x cell lysis buffer (#9803, Cell signaling). Protease and phosphatase inhibitors (Roche) were added to all

buffers. For immunoprecipitation experiments, HEK293 cells were transiently co-transfected with Flag-HDAC9 and the specific component of the NF- κ B pathway under assessment: HA-IKK β (In vivoGen); HA-IKK α (In vivoGen); HA-IKK γ ; HA-I κ B α ; HA-GSK3 β or HA-RSK1. pcDNA3 HA human NEMO was a gift from Kunliang Guan (Addgene plasmid # 13512). pCMV4-3 HA/I κ B- α was a gift from Warner Greene (Addgene plasmid # 21985). HA GSK3 beta wt pcDNA3 was a gift from Jim Woodgett (Addgene plasmid # 14753). pKH3-human RSK1 was a gift from John Blenis (Addgene plasmid # 13841). Cells were treated with 1 μ M MG132 for 1 h to prevent proteasomal degradation prior to lysis. Following incubation of 250 μ g of protein with 10 μ g of primary antibody (anti-Flag or anti-HA) overnight at 4°C, the ensuing protein complexes were incubated with protein A or G beads for 2 h. Antibody-antigen complexes were eluted from the beads after washing with 1x cell lysis buffer containing 150 mM NaCl and a final stringent wash with 250 mM NaCl. For subcellular fractionation, nuclear extracts were isolated using a subcellular fractionation kit following the manufacturer's protocol (Active Motif). Total cell lysates, nuclear extracts or coimmunoprecipitated proteins were separated by SDS-PAGE, transferred to a PVDF membrane (Bio-Rad), and detected with the appropriate antibodies. Primary antibodies were incubated overnight at 4°C. HRP-conjugated anti-mouse or anti-rabbit antibodies were used as secondary antibodies and blots were developed with Immobilon Western HRP Substrate (Merck Millipore). Protein bands were visualized with a Fusion Fx7 and quantified using Image J 1.47v software (Wayne Rasband).

Kinase activity assay

HEK293 cells were transfected with either Flag-HDAC9 and HA-IKK β or Flag-alone and HA-IKK β and subsequently lysed in ice-cold 1x cell lysis buffer (#9803, Cell Signaling) supplemented

with protease and phosphatase inhibitors. Immunoprecipitation of IKK β and HDAC9 were performed as described above with anti-HA and anti-Flag antibody, respectively. The immunoprecipitated complexes were washed three times with ice-cold 1x cell lysis buffer and three times with ice-cold 1x kinase buffer (#9802, Cell Signaling). Thereafter, the complexes were incubated with recombinant p65 (400 ng) as substrate at 34°C for 45 min in the presence of 100 μ M ATP. Reactions were stopped by the addition of 4x Laemmli sample buffer followed by incubation at 95°C for 20 min. Proteins were separated on 7% SDS-PAGE and immunoblotted for p65 phosphorylation using anti-NF- κ B p65 (phospho S536) antibody.

Confocal microscopy

HUVECs were transfected with *HDAC9* siRNA or scrambled control RNA and stimulated at different time intervals with TNF- α . Cells were washed with 1x PBS, fixed with 4% PFA-PBS solution for 10 minutes and permeabilized using 0.1% Triton X. Cells were then blocked for 1 h with 0.2% FCS, 0.2% BSA and 0.002% fish skin gelatin in 1x PBS. In the same solution, the primary antibody for p65 was incubated overnight at 4°C. DAPI and Alexa Fluor 488-labeled secondary antibodies were incubated for 1 h at room temperature. Cells were washed and sealed with a coverslip coated in fluoromount mounting medium (Sigma). Imaging was performed with the confocal microscope (LSM 880, Zeiss) using the 40x oil objective and analyzed with the ZEN software (Zeiss).

Statistical Analysis

Statistical analysis was performed with GraphPad Prism 6 (GraphPad Software Inc.). Data are represented as means \pm s.e.m. After testing for normality, data were analyzed by two-tailed

unpaired Student's t test or Mann–Whitney test or Fisher's exact test, one-way or two-way ANOVA with Bonferroni or Holm-Sidak multiple comparison test or Fisher's LSD test or Kruskal-Wallis with Dunn's multiple comparison test, as appropriate. P values <0.05 were considered to be statistically significant.

Results

Hdac9 promotes pro-inflammatory responses and enhances features of atherosclerotic plaque vulnerability

To study the role of Hdac9 in vascular inflammation, we used mouse models of atherosclerosis. Lethally irradiated *ApoE*^{-/-} mice were reconstituted with bone marrow from either *Hdac9*^{+/+}*ApoE*^{-/-} (*Hdac9*^{+/+} BM) or *Hdac9*^{-/-}*ApoE*^{-/-} mice (*Hdac9*^{-/-} BM) and were fed a Western-type diet for 11 weeks followed by analysis of aortic root lesions (**Fig. 1a**). Reconstitution with *Hdac9*-deficient bone marrow was atheroprotective with smaller lesion sizes and a lower proportion of advanced lesions compared to control bone marrow (**Fig. 1b-d**), while lipid levels, body weight, and circulating leukocyte counts did not differ between groups (**table S1**). To determine features of plaque vulnerability we focused on advanced lesions. *Hdac9* deficiency in hematopoietic cells lowered lesional macrophage content and necrotic core size and increased fibrous cap thickness thus reducing overall plaque vulnerability (**Fig. 1e-j and fig. S1a-c**). Moreover, *Hdac9*-deficient bone marrow-derived macrophages (BMDMs) showed reduced TNF α -induced upregulation of pro-inflammatory cytokines and chemokines on mRNA and protein level (**Fig. 1k-m**). Collectively, these findings indicate that Hdac9 promotes pro-inflammatory responses in the bone marrow-derived compartment of the vasculature and enhances features of atherosclerotic plaque vulnerability.

HDAC9 binds to IKK α and IKK β resulting in their deacetylation and activation

The mechanisms linking HDAC9 to vascular inflammation and plaque instability are unknown. In light of the central role of NF- κ B in atherosclerosis and the resemblance of HDAC9-related inflammatory gene expression with NF- κ B-driven transcriptional responses²³, we hypothesized that NF- κ B might be a downstream effector of HDAC9 (**Fig. 2a**). Co-immunoprecipitation experiments revealed a complex involving HDAC9, IKK α , and IKK β but not IKK γ , I κ B α , and the non-canonical kinases GSK3 β and RSK1 (**Fig. 2b** and **fig. S2a**). Of note, we detected IKK α and IKK β upon HDAC9 pulldown and *vice versa* (**fig. S2b, c**). To investigate the functional consequence of these interactions, we determined the acetylation status of IKK α and IKK β and found reduced acetylation of both kinases in the presence of HDAC9 (**Fig. 2c, d**). This was accompanied by enhanced activity of IKK β as evidenced by increased phosphorylation of p65 in the presence of HDAC9 in an *in vitro* kinase activity assay (**Fig. 2e** and **fig. S2d**) in accord with the established inhibitory effect of acetylation on IKK activation²⁴. IKK β phosphorylates p65 at serine residues 536 and 468, while IKK α phosphorylates p65 at 536²⁵. We therefore examined the effect of HDAC9 on p65 phosphorylation at these residues as an endogenous readout for the activation of IKK. Indeed, *Hdac9*-deficient BMDMs showed reduced Tnf- α -induced phosphorylation at both serine 536 and 468 (**Fig. 2f, g**). Given the pivotal role of NF- κ B in driving pro-inflammatory responses in the vascular endothelium, we extended our findings to endothelial cells. siRNA-mediated knockdown of *HDAC9* in human umbilical vein endothelial cells (HUVECs) likewise reduced p65 phosphorylation at serine 536 and 468 without affecting phosphorylation at serine 276 (**Fig. 2h, i**) which is mediated by MSK1, PIM1, and PKAc²⁵. In contrast, we found no effect of HDAC9 on ERK1/2 and p38MAPK signaling (**fig. S3a-d**), further corroborating the specificity of the downstream signaling events induced by HDAC9/IKK

interactions. The reduced phosphorylation of p65 upon *HDAC9* knockdown was accompanied by reduced nuclear localization of p65 (**Fig. 2j-l and fig. S3e, f**) and a subsequent decrease in *de novo* synthesis of I κ B- α (**fig. S4a-d**). Consequently, the expression of prototypical NF- κ B -driven pro-inflammatory target genes was reduced both in *HDAC9*-depleted HUVECs and in *Hdac9*-deficient mice (**Fig. 2m and fig. S5a-l**). Collectively, these findings define the IKK/NF- κ B pathway as a major downstream effector linking HDAC9 to vascular inflammation.

Pharmacological inhibition with TMP195 attenuates the initiation of atherosclerosis

To assess the therapeutic implication of our observations, we utilized TMP195, a selective class IIa HDAC inhibitor with high affinity for HDAC9^{22, 26}, in a mouse model of atherogenesis constituting important features of endothelial activation and myeloid cell recruitment. *ApoE*^{-/-} mice were fed Western-type diet for 4 weeks and in parallel received TMP195 or vehicle (**Fig. 3a**). TMP195 attenuated early lesion formation (**Fig. 3b, c**) and reduced endothelial activation as demonstrated by mitigated Vcam-1 expression (**Fig. 3d, e and fig. S6a**). Accordingly, the invasion of monocytes and neutrophils into atherosclerotic lesions was reduced in TMP195-treated mice (**Fig. 3f, g and fig. S6b, c**) likely attributable to impaired leukocyte-endothelial interactions as demonstrated by a reduction of myeloid cell rolling and adhesion to carotid arteries (**Fig. 3h-k and fig. S6d-f**). Hence, treatment with TMP195 confers atheroprotection by limiting leukocyte recruitment into atherosclerotic lesions.

TMP195 limits pro-inflammatory responses consistent with reduced activation of IKK β

NF- κ B takes center stage in regulating adhesion molecules and chemokines involved in leukocyte-endothelial interactions at the vascular wall ²³. Given our findings on the activating effect of HDAC9 on NF- κ B (Fig. 2), we examined the consequence of TMP195 treatment on NF- κ B activity. TMP195 enhanced the acetylation (**Fig. 4a, b**) and reduced the activity of IKK β as demonstrated by reduced phosphorylation of p65 in HEK293 cells, and in BMDMs (**Fig. 4c-e**). Accordingly, TMP195 inhibited NF- κ B-driven cytokine and chemokine expression, which have established roles in vascular inflammation (**Fig. 4f**), thus essentially paralleling our data upon gene silencing of *Hdac9* (Fig. 2m). The prominent inhibitory effect of TMP195 on pro-inflammatory responses in macrophages prompted us to examine the transcriptome of TMP195-treated BMDMs stimulated with Tnf- α . Gene expression profiling showed that TMP195 downregulated key inflammatory pathways including ‘cell surface interactions at the vascular wall’ and ‘cytokine signaling in immune system’ (**Fig. 4g**). Moreover, out of 272 differentially regulated genes in TMP195-treated BMDMs, 85 overlapped with those induced by treatment with the IKK β inhibitor TPCA-1 ²⁷ with consistent directionality in 86% (73/85) of overlapping genes (**Fig. 4h** and **fig. S7a**). Further analysis revealed that co-treatment with both inhibitors had no additive effect on cytokine and chemokine expression (**Fig. 4i**), consistent with the hypothesis that the anti-inflammatory effects of TMP195 are mediated, at least in part, through inhibitory effects on IKK β .

Therapeutic inhibition with TMP195 reduces atheroprogession and confers plaque stability

Preventive treatment in patients at risk for cardiovascular disease is typically initiated at a stage when lesions already exist. Hence, we explored the therapeutic effects of TMP195 on established atherosclerosis. *ApoE*^{-/-} mice receiving Western-type diet for 8 weeks were treated with TMP195

or vehicle starting from the 5th week of diet, when lesions had developed (**Fig. 5a**). TMP195 attenuated the progression of established atherosclerosis as revealed by a reduction of lesion sizes in comparison with vehicle-treated mice (**Fig. 5b, c** and **fig. S7b-d**). TMP195 further reduced the invasion of classical monocytes and neutrophils into atherosclerotic lesions (**Fig. 5d** and **fig. S7e**). Importantly, TMP195 exhibited pronounced atheroprotective effects even at later stages when initiating treatment from the 8th week of diet (**Fig. 5e**). TMP195 attenuated advanced lesion size, reduced necrotic core formation, and increased fibrous cap thickness along with a trend for increased smooth muscle cell content resulting in a more stable plaque phenotype (**Fig. 5f - k** and **fig. S8 a-c**). This was consistent with reduced NF- κ B target gene expression in advanced lesions in TMP195-treated mice (**Fig. 5l**). Hence, aside from exerting beneficial effects on early atherogenesis, TMP195 attenuates progression of existing atherosclerotic lesions and confers plaque stability.

Given the effects of TMP195 on vascular inflammation and atheroprogession as well as plaque stability in mice, we further analyzed the activation of monocytes from patients with atherosclerosis (**Fig. 5m** and **table S2**). Specifically, we determined the effect of *ex vivo* treatment with TMP195 or vehicle on phosphorylation of p65 and cytokine production after stimulation with TNF- α . TMP195 reduced phosphorylation of p65 at serine 536 resulting in a significantly reduced production of cytokines and chemokines including IL-1 β and IL-6 (**Fig. 5n-p**). Collectively, these results demonstrate that therapeutic inhibition with TMP195 induces a stable plaque phenotype in mice and limits the activation of monocytes from patients with atherosclerosis.

Discussion

Our findings provide a mechanistic explanation for the prominence of HDAC9 as a vascular risk locus in genome-wide association studies (GWAS) and suggest that therapeutic targeting of HDAC9 may provide a potent strategy for preventing vascular inflammation. This conclusion is supported by i) the increase in atherosclerotic plaque stability conferred by genetic depletion of *Hdac9* as well as pharmacological inhibition with class IIa HDACi; ii) the activating effect of HDAC9 on IKK in macrophages and vascular endothelial cells; and iii) the reduced activation of monocytes from patients with atherosclerosis upon *ex vivo* inhibition of this HDAC9-dependent pathway by treatment with small molecule inhibitor TMP195.

Inflammatory and immune responses are governed by mechanisms of transcriptional regulation²⁸⁻³² and modulating these mechanisms may limit vascular inflammation. HDAC inhibitors are powerful transcriptional regulators that are in clinical use for some conditions including T cell lymphoma^{7, 33}. Yet, broad-spectrum HDAC inhibitors (HDACi) have contraindications limiting their application in cardiovascular disease^{33, 34}. In fact, treatment with trichostatin A has been shown to exacerbate atherosclerotic lesion size³⁴ despite an anti-atherogenic function in M ϕ ³⁵. This might relate to distinct and even opposing roles of individual HDACs in atherosclerosis^{12, 21, 36, 37} or differential actions of broad-spectrum HDACi on individual HDACs. Our findings reveal vascular protective effects of class IIa HDAC inhibition with TMP195 thus overcoming a central limitation to the use of broad-spectrum HDACi³⁴. Whether further restricting the inhibitory activity to individual HDACs³³ or specifically targeting M ϕ ³⁶ and ECs^{37, 38}, for instance by nano-delivery strategies³⁹, would confer additional benefit remains to be shown.

The previously unrecognized activating effect of HDAC9 on NF- κ B signaling as unraveled here offers a strategy for fine-tuning NF- κ B responses to reduce vascular inflammation^{19, 40, 41}. This involves HDAC9-mediated deacetylation and subsequent activation of IKK potentially as part of a larger molecular complex. NF- κ B signaling is modulated by phosphorylation of its subunits. Phosphorylation of p65 either transactivates or inhibits NF- κ B activity depending on the kinases and specific residues involved. IKK phosphorylates p65 at serine 536 and 468, enhances transactivation, and directs transcription in a target gene-specific manner^{42,43}. Of note, our finding that HDAC9 is required for sustained p65 phosphorylation at serines 536 and 468 fits with the pattern of reduced inflammatory cytokines, chemokines, and adhesion molecules demonstrated here in various experimental paradigms of HDAC9 inactivation or depletion.

Drug targets with support from human genetics have a higher probability of reaching phase III clinical trials and regulatory approval^{44, 45}. GWAS in a broad range of vascular conditions¹⁴⁻¹⁸ highlight an exceptional role of the *HDAC9* region in major complications of human atherosclerosis. As such, our current findings in mice and in isolated cells including human monocytes provide triangulation of evidence⁴⁶ for HDAC9 as a causal factor in atherosclerosis and a promising target for interventional studies in humans. The inhibitory effect of TMP195 on the secretion of inflammatory cytokines including IL-1 β and IL-6 in monocytes from patients with atherosclerosis would further agree with the concept of targeting the residual inflammatory risk in high-risk populations^{47, 48}.

Treatment with TMP195 limited features of plaque vulnerability consistent with results obtained in *Hdac9*-deficient mice. As a potential limitation, our animal models do not fully reflect the phenotype of human atherosclerotic plaques, which includes plaque destabilization and rupture with occlusive thrombosis. Also, developing class IIa HDAC inhibitors with even higher

specificity for HDAC9 may be needed to exploit the full potential of HDAC9 inhibition for the prevention of atherosclerosis.

In summary, we demonstrate that HDAC9 promotes pro-inflammatory responses in the vasculature to augment features of atherosclerotic plaque vulnerability. HDAC9 binds to IKK α and β resulting in their deacetylation and subsequent activation, which drives vascular inflammation. Treatment with TMP195, a selective class IIa HDAC inhibitor, inhibits key inflammatory pathways, attenuates atherogenesis, atheroprogession, and late-stage atherosclerosis, and confers plaque stability, thus defining a novel therapeutic strategy to reduce the burden of vascular inflammation.

References

1. Herrington W, Lacey B, Sherliker P, Armitage J and Lewington S. Epidemiology of Atherosclerosis and the Potential to Reduce the Global Burden of Atherothrombotic Disease. *Circ Res.* 2016;118:535-46.
2. Weber C and Noels H. Atherosclerosis: current pathogenesis and therapeutic options. *Nat Med.* 2011;17:1410-22.
3. Libby P, Lichtman AH and Hansson GK. Immune effector mechanisms implicated in atherosclerosis: from mice to humans. *Immunity.* 2013;38:1092-104.
4. Moore KJ, Sheedy FJ and Fisher EA. Macrophages in atherosclerosis: a dynamic balance. *Nat Rev Immunol.* 2013;13:709-21.
5. Silvestre-Roig C, de Winther MP, Weber C, Daemen MJ, Lutgens E and Soehnlein O. Atherosclerotic plaque destabilization: mechanisms, models, and therapeutic strategies. *Circ Res.* 2014;114:214-26.
6. Shakespear MR, Halili MA, Irvine KM, Fairlie DP and Sweet MJ. Histone deacetylases as regulators of inflammation and immunity. *Trends Immunol.* 2011;32:335-43.
7. Falkenberg KJ and Johnstone RW. Histone deacetylases and their inhibitors in cancer, neurological diseases and immune disorders. *Nat Rev Drug Discov.* 2014;13:673-91.
8. Tao R, de Zoeten EF, Ozkaynak E, Chen C, Wang L, Porrett PM, Li B, Turka LA, Olson EN, Greene MI, Wells AD and Hancock WW. Deacetylase inhibition promotes the generation and function of regulatory T cells. *Nat Med.* 2007;13:1299-307.
9. Lapiere M, Linares A, Dalvai M, Duraffourd C, Bonnet S, Boulahtouf A, Rodriguez C, Jalaguier S, Assou S, Orsetti B, et al., Histone deacetylase 9 regulates breast cancer cell proliferation and the response to histone deacetylase inhibitors. *Oncotarget.* 2016;7:19693-708.
10. Kaluza D, Kroll J, Gesierich S, Manavski Y, Boeckel JN, Doebele C, Zelent A, Rossig L, Zeiher AM, Augustin HG, Urbich C and Dimmeler S. Histone deacetylase 9 promotes angiogenesis by targeting the antiangiogenic microRNA-17-92 cluster in endothelial cells. *Arterioscler Thromb Vasc Biol.* 2013;33:533-43.
11. Cao Q, Rong S, Repa JJ, St Clair R, Parks JS and Mishra N. Histone deacetylase 9 represses cholesterol efflux and alternatively activated macrophages in atherosclerosis development. *Arterioscler Thromb Vasc Biol.* 2014;34:1871-9.
12. Chen J, Wang N, Dong M, Guo M, Zhao Y, Zhuo Z, Zhang C, Chi X, Pan Y, Jiang J, et al., The Metabolic Regulator Histone Deacetylase 9 Contributes to Glucose Homeostasis Abnormality Induced by Hepatitis C Virus Infection. *Diabetes.* 2015;64:4088-98.
13. International Stroke Genetics C, Wellcome Trust Case Control C, Bellenguez C, Bevan S, Gschwendtner A, Spencer CC, Burgess AI, Pirinen M, Jackson CA, Traylor M, Strange A, Su Z, et al., Genome-wide association study identifies a variant in HDAC9 associated with large vessel ischemic stroke. *Nat Genet.* 2012;44:328-33.
14. Malik R, Chauhan G, Traylor M, Sargurupremraj M, Okada Y, Mishra A, Rutten-Jacobs L, Giese AK, van der Laan SW, Gretarsdottir S, et al., Multiancestry genome-wide association study of 520,000 subjects identifies 32 loci associated with stroke and stroke subtypes. *Nat Genet.* 2018;50:524-537.
15. Consortium CAD, Deloukas P, Kanoni S, Willenborg C, Farrall M, Assimes TL, Thompson JR, Ingelsson E, Saleheen D, Erdmann J, Goldstein BA, et al., Large-scale

- association analysis identifies new risk loci for coronary artery disease. *Nat Genet.* 2013;45:25-33.
16. Malhotra R, Mauer AC, Lino Cardenas CL, Guo X, Yao J, Zhang X, Wunderer F, Smith AV, Wong Q, Pechlivanis S, et al., HDAC9 is implicated in atherosclerotic aortic calcification and affects vascular smooth muscle cell phenotype. *Nat Genet.* 2019.
 17. Klarin D, Lynch J, Aragam K, Chaffin M, Assimes TL, Huang J, Lee KM, Shao Q, Huffman JE, Natarajan P, et al., Genome-wide association study of peripheral artery disease in the Million Veteran Program. *Nat Med.* 2019;25:1274-1279.
 18. Asare Y, Ommer M, Azombo FA, Alampour-Rajabi S, Sternkopf M, Sanati M, Gijbels MJ, Schmitz C, Sinitiski D, Tilstam PV, et al., Inhibition of atherogenesis by the COP9 signalosome subunit 5 in vivo. *Proc Natl Acad Sci U S A.* 2017;114:E2766-E2775.
 19. Silvestre-Roig C, Braster Q, Wichapong K, Lee EY, Teulon JM, Berrebeh N, Winter J, Adrover JM, Santos GS, Froese A, et al., Externalized histone H4 orchestrates chronic inflammation by inducing lytic cell death. *Nature.* 2019;569:236-240.
 20. Azghandi S, Prell C, van der Laan SW, Schneider M, Malik R, Berer K, Gerdes N, Pasterkamp G, Weber C, Haffner C and Dichgans M. Deficiency of the stroke relevant HDAC9 gene attenuates atherosclerosis in accord with allele-specific effects at 7p21.1. *Stroke.* 2015;46:197-202.
 21. Guerriero JL, Sotayo A, Ponichtera HE, Castrillon JA, Pourzia AL, Schad S, Johnson SF, Carrasco RD, Lazo S, Bronson RT, Davis SP, Lobera M, Nolan MA and Letai A. Class IIa HDAC inhibition reduces breast tumours and metastases through anti-tumour macrophages. *Nature.* 2017;543:428-432.
 22. de Winther MP, Kanters E, Kraal G and Hofker MH. Nuclear factor kappaB signaling in atherogenesis. *Arterioscler Thromb Vasc Biol.* 2005;25:904-14.
 23. Mittal R, Peak-Chew SY and McMahon HT. Acetylation of MEK2 and I kappa B kinase (IKK) activation loop residues by YopJ inhibits signaling. *Proc Natl Acad Sci U S A.* 2006;103:18574-9.
 24. Hoesel B and Schmid JA. The complexity of NF-kappaB signaling in inflammation and cancer. *Mol Cancer.* 2013;12:86.
 25. Lobera M, Madauss KP, Pohlhaus DT, Wright QG, Trocha M, Schmidt DR, Baloglu E, Trump RP, Head MS, Hofmann GA, et al., Selective class IIa histone deacetylase inhibition via a nonchelating zinc-binding group. *Nat Chem Biol.* 2013;9:319-25.
 26. Betancur PA, Abraham BJ, Yiu YY, Willingham SB, Khameneh F, Zarnegar M, Kuo AH, McKenna K, Kojima Y, Leeper NJ, et al., A CD47-associated super-enhancer links pro-inflammatory signalling to CD47 upregulation in breast cancer. *Nat Commun.* 2017;8:14802.
 27. Chen L, Fischle W, Verdin E and Greene WC. Duration of nuclear NF-kappaB action regulated by reversible acetylation. *Science.* 2001;293:1653-7.
 28. Christ A, Gunther P, Lauterbach MAR, Duewell P, Biswas D, Pelka K, Scholz CJ, Oosting M, Haendler K, et al., Western Diet Triggers NLRP3-Dependent Innate Immune Reprogramming. *Cell.* 2018;172:162-175 e14.
 29. Li X, Zhang Q, Ding Y, Liu Y, Zhao D, Zhao K, Shen Q, Liu X, Zhu X, Li N, Cheng Z, Fan G, Wang Q and Cao X. Methyltransferase Dnmt3a upregulates HDAC9 to deacetylate the kinase TBK1 for activation of antiviral innate immunity. *Nat Immunol.* 2016;17:806-15.

30. Lino Cardenas CL, Kessinger CW, Cheng Y, MacDonald C, MacGillivray T, Ghoshhajra B, Huleihel L, Nuri S, Yeri AS, Jaffer FA, et al., An HDAC9-MALAT1-BRG1 complex mediates smooth muscle dysfunction in thoracic aortic aneurysm. *Nat Commun.* 2018;9:1009.
31. Kuznetsova T, Prange KHM, Glass CK and de Winther MPJ. Transcriptional and epigenetic regulation of macrophages in atherosclerosis. *Nat Rev Cardiol.* 2019.
32. Neele AE, Van den Bossche J, Hoeksema MA and de Winther MP. Epigenetic pathways in macrophages emerge as novel targets in atherosclerosis. *Eur J Pharmacol.* 2015;763:79-89.
33. Choi JH, Nam KH, Kim J, Baek MW, Park JE, Park HY, Kwon HJ, Kwon OS, Kim DY and Oh GT. Trichostatin A exacerbates atherosclerosis in low density lipoprotein receptor-deficient mice. *Arterioscler Thromb Vasc Biol.* 2005;25:2404-9.
34. Van den Bossche J, Neele AE, Hoeksema MA, de Heij F, Boshuizen MC, van der Velden S, de Boer VC, Reedquist KA and de Winther MP. Inhibiting epigenetic enzymes to improve atherogenic macrophage functions. *Biochem Biophys Res Commun.* 2014;455:396-402.
35. Hoeksema MA, Gijbels MJ, Van den Bossche J, van der Velden S, Sijm A, Neele AE, Seijkens T, Stoger JL, Meiler S, Boshuizen MC, et al., Targeting macrophage Histone deacetylase 3 stabilizes atherosclerotic lesions. *EMBO Mol Med.* 2014;6:1124-32.
36. Zampetaki A, Zeng L, Margariti A, Xiao Q, Li H, Zhang Z, Pepe AE, Wang G, Habi O, deFalco E, Cockerill G, Mason JC, Hu Y and Xu Q. Histone deacetylase 3 is critical in endothelial survival and atherosclerosis development in response to disturbed flow. *Circulation.* 2010;121:132-42.
37. Zhou B, Margariti A, Zeng L and Xu Q. Role of histone deacetylases in vascular cell homeostasis and arteriosclerosis. *Cardiovasc Res.* 2011;90:413-20.
38. Lameijer M, Binderup T, van Leent MMT, Senders ML, Fay F, Malkus J, Sanchez-Gaytan BL, Teunissen AJP, Karakatsanis N, Robson P, et al., Efficacy and safety assessment of a TRAF6-targeted nanoimmunotherapy in atherosclerotic mice and non-human primates. *Nat Biomed Eng.* 2018;2:279-292.
39. Taniguchi K and Karin M. NF-kappaB, inflammation, immunity and cancer: coming of age. *Nat Rev Immunol.* 2018;18:309-324.
40. Reissig S, Tang Y, Nikolaev A, Gerlach K, Wolf C, Davari K, Gallus C, Masri J, Mufazalov IA, Neurath MF, Wunderlich FT, Schattenberg JM, Galle PR, Weigmann B, Waisman A, Glasmacher E and Hovelmeier N. Elevated levels of Bcl-3 inhibits Treg development and function resulting in spontaneous colitis. *Nat Commun.* 2017;8:15069.
41. Christian F, Smith EL and Carmody RJ. The Regulation of NF-kappaB Subunits by Phosphorylation. *Cells.* 2016;5.
42. Moreno R, Sobotzik JM, Schultz C and Schmitz ML. Specification of the NF-kappaB transcriptional response by p65 phosphorylation and TNF-induced nuclear translocation of IKK epsilon. *Nucleic Acids Res.* 2010;38:6029-44.
43. Nelson MR, Tipney H, Painter JL, Shen J, Nicoletti P, Shen Y, Floratos A, Sham PC, Li MJ, Wang J, Cardon LR, Whittaker JC and Sanseau P. The support of human genetic evidence for approved drug indications. *Nat Genet.* 2015;47:856-60.
44. Finan C, Gaulton A, Kruger FA, Lumbers RT, Shah T, Engmann J, Galver L, Kelley R, Karlsson A, Santos R, Overington JP, Hingorani AD and Casas JP. The druggable genome

- and support for target identification and validation in drug development. *Sci Transl Med.* 2017;9.
45. Munafo MR and Davey Smith G. Robust research needs many lines of evidence. *Nature.* 2018;553:399-401.
 46. Ridker PM, Everett BM, Thuren T, MacFadyen JG, Chang WH, Ballantyne C, Fonseca F, Nicolau J, Koenig W, Anker SD, et al., Antiinflammatory Therapy with Canakinumab for Atherosclerotic Disease. *N Engl J Med.* 2017;377:1119-1131.
 47. Ridker PM. Clinician's Guide to Reducing Inflammation to Reduce Atherothrombotic Risk: JACC Review Topic of the Week. *J Am Coll Cardiol.* 2018;72:3320-3331.

Acknowledgements: We thank Farida Hellal for discussions and help with confocal imaging. Flavia Söllner for help with generating Flag-HDAC9 construct. Helmut Blum and Stefan Krebs for RNA-sequencing.

Funding: This work was supported by grants from the Deutsche Forschungsgemeinschaft (DFG) (CRC 1123 [B3] and Munich Cluster for Systems Neurology [SyNergy]), the German Federal Ministry of Education and Research (BMBF, e:Med programme e:AtheroSysMed), the FP7/2007-2103 European Union project CVgenes@target (grant agreement No Health-F2-2013-601456), the European Union Horizon2020 project SVDs@target (grant agreement No 66688), the Vascular Dementia Research Foundation, and the Corona Foundation to MD. Y. A was supported by grants from the Deutsche Forschungsgemeinschaft (CRC 1123 [B3], the FöFoLe program of Ludwig-Maximilians University Munich (FöFoLe 921) and by the Friedrich Baur Stiftung. O. S. receives support from the Deutsche Forschungsgemeinschaft (CRC 914 [B8], CRC 1123 [A6] [B5], SO876/11-1), the Vetenskapradet, the Else Kröner Fresenius Stiftung and the Leducq Foundation. J.B. received funding from DFG/CRC 1123 [A3] and DFG under Germany's Excellence Strategy within the framework of the Munich Cluster for Systems Neurology (EXC 2145 SyNergy – ID 390857198). S.T. was supported by the Josef-Hackl-Stiftung. R.T.A.M. and two-photon

microscopic experiments are supported by the Deutsche Forschungsgemeinschaft (CRC1123 [Z01] and INST409/97-1 FUGG).

Disclosures: The authors declare that they have no competing interests

Supplemental Materials

Supplemental Table 1-4

Supplemental Figures Legends

Supplemental Figures 1-8

Figure Legends

Fig. 1. Hdac9 promotes pro-inflammatory responses and enhances atherosclerotic plaque vulnerability. **a – j**, Experimental outline. Lethally irradiated *ApoE*^{-/-} mice were reconstituted with bone marrow from either *Hdac9*^{-/-}*ApoE*^{-/-} (*Hdac9*^{-/-} BM) or *Hdac9*^{+/+}*ApoE*^{-/-} (*Hdac9*^{+/+} BM) mice and were fed a Western-type diet for 11 weeks to induce advanced atherosclerosis (**a**). **b**, Representative image of Oil-Red-O stained aortic root lesion. Scale bars, 200 μ m. **c**, Quantification of lesion sizes. **d**, Lesion classification on Masson Trichrome stained sections. Two-sided Mann-Whitney test (**c**) and two-sided Fisher's exact test (**d**). Quantification of necrotic core area (**e**), representative immunostainings (**f**) showing lesional CD68⁺ macrophage area in red and SMA⁺ smooth muscle cell area in green. Scale bars, 100 μ m. **g**) Quantification of macrophage area. **h**, Overall vulnerability. **i**, Representative Masson Trichrome stained lesions with fibrous cap (FC) indicated with arrow heads. Scale bars, 50 μ m. **j**, Quantification of FC thickness. Two-sided unpaired t-test. **k – m**, BMDMs isolated from *Hdac9*^{-/-}*ApoE*^{-/-} and *Hdac9*^{+/+}*ApoE*^{-/-} mice were either stimulated with Tnf- α (50 ng/ml) or left untreated (**k**). Quantification of gene expression (after 6 h of Tnf- α stimulation; **l**) and secretion (after 24 h of Tnf- α stimulation; **m**) of key pro-inflammatory chemokines and cytokines. Two-way Anova with Bonferroni correction. Data are mean \pm s.e.m.

Fig. 2. HDAC9 binds to IKK α and IKK β resulting in their deacetylation and activation. **a**, Schematic representation of the canonical NF- κ B pathway. **b – e**, HEK293 cells were transiently co-transfected with Flag-HDAC9 and individual components of the IKK complex (HA-IKK α ; HA-IKK β ; or HA-IKK γ). **b**, Representative immunoblots depicting the interaction between HDAC9 and IKK. n=2-4 independent experiments. **c**, Representative immunoblots of acetylated

IKK α and IKK β and their non-acetylated forms. **d**, Quantification of acetylated IKK α and IKK β normalized to non-acetylated forms. Two-sided Mann–Whitney test. **e**, Representative immunoblots of kinase activity assay. n=2 independent experiments. **f**, Representative immunoblots showing p65 phosphorylation at serine residues 536 and 468, and corresponding non-phosphorylated forms in Tnf- α -stimulated *Hdac9*-deficient versus control BMDMs. **g**, Quantification of p-p65 (S536, 45 min; and S468, 5 min of Tnf- α stimulation) normalized to total p65. Two-sided unpaired t-test. **h – m**, HUVECs were transiently transfected with *HDAC9* siRNA or scrambled control (*SCR*) RNA for 72 h and subsequently stimulated with TNF- α (20 ng/mL) for indicated periods or left untreated. **h**, Representative immunoblots showing p65 phosphorylation at serine residues 536, 468, and 276 and corresponding non-phosphorylated forms. **i**, Quantification of p-p65 (S536, 120 min; and S468, 5 min of Tnf- α stimulation) normalized to total p65. Two-sided unpaired t-test (S536) and two-sided Mann–Whitney test (S468). **j**, Determination of nuclear localization of p65 by confocal microscopy. Shown are representative immunostainings of three independent experiments. Scale bar, 10 μ m. **k**, Representative immunoblots of nuclear p65 and lamin B1. **l**, Quantification of nuclear p65 normalized to lamin B1. Two-way Anova with Bonferroni correction. **m**, Gene expression analysis by RT-PCR after 8 h of TNF- α stimulation. Two-way Anova with Bonferroni correction. Data are mean \pm s.e.m.

Fig. 3. TMP195 attenuates the initiation of atherosclerosis. **a – g**, Experimental outline. *ApoE*^{-/-} mice were fed Western-type diet for 4 weeks and in parallel received TMP195 (50 mg/Kg) or vehicle (**a**). **b**, Representative Oil-Red-O stained aortic root lesion. Scale bars, 200 μ m. **c**, Quantification of lesion sizes. Two-sided unpaired t-test. **d**, Representative immunostaining of

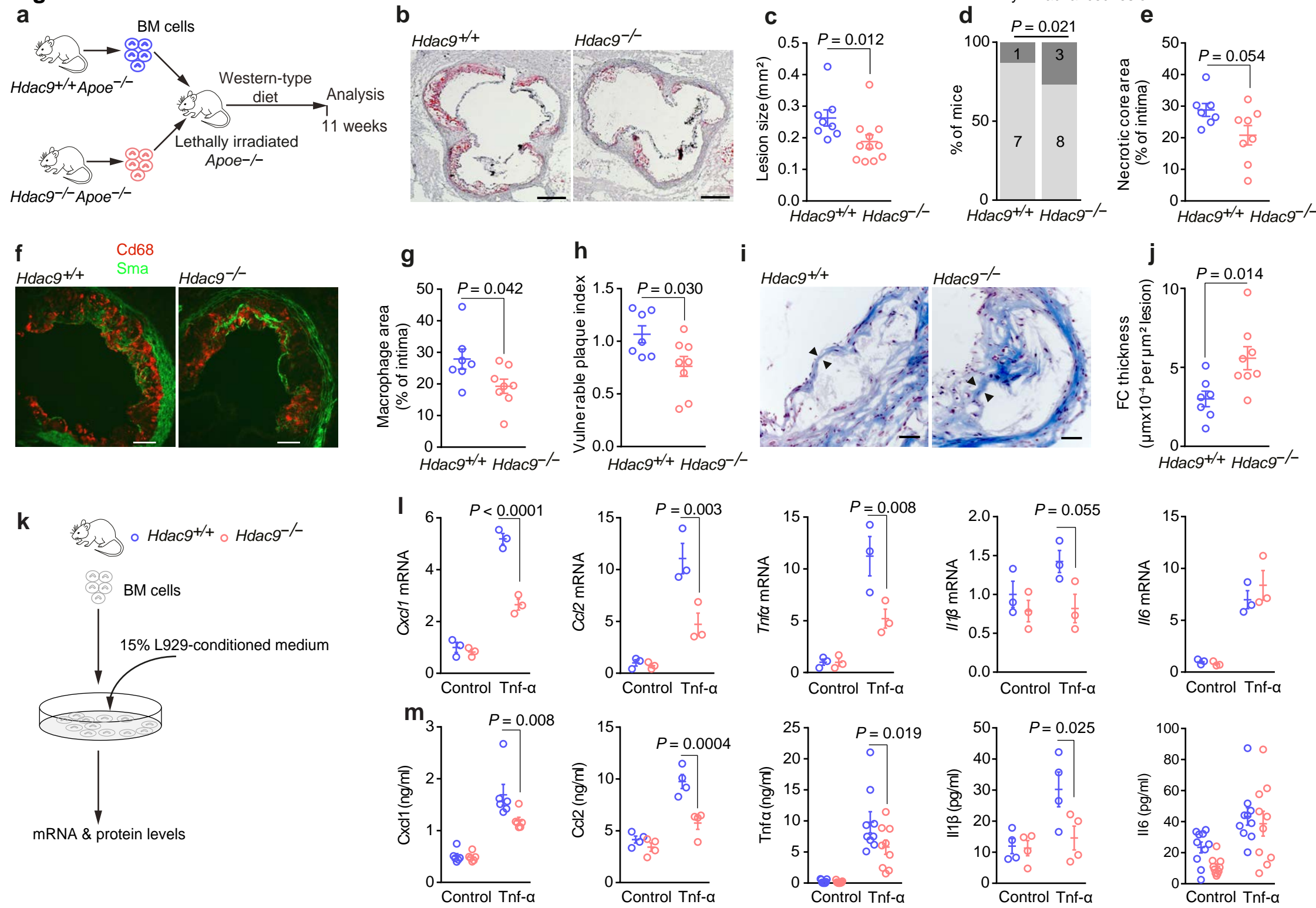
Vcam-1 in carotid arteries visualized by two-photon microscopy. Scale bars, 50 μm . **e**, Quantification of Vcam-1 expression. Two-sided Mann–Whitney test. **f, g**, Analysis of leukocyte accumulation in atherosclerotic aortas by flow cytometry. Quantification of aortic Ly6C^{high} monocytes **f**) and aortic Ly6G⁺ cells **g**). Two-sided unpaired t-test. **h – k**, *Cx3cr1^{gfp/wt}Apoe^{-/-}* mice were fed a Western-type diet for 4 weeks, and in parallel received TMP195 (50 mg/kg) or vehicle. Examination of leukocyte-endothelial interaction by intravital microscopy. Representative image of CD11b⁺ adhesion **h**). Scale bars, 100 μm . Quantification of adherent CD11b⁺ cells **i**), adherent Ly6C⁺ cells **j**), and adherent Ly6G⁺ cells **k**). Two-sided unpaired t-test. Data are mean \pm s.e.m.

Fig. 4. TMP195 limits pro-inflammatory responses consistent with reduced activation of IKK β . **a, b**, Following transfection of IKK β , HEK293 cells were treated with vehicle or TMP195. **a**, Representative immunoblots of acetylated and total IKK β . **b**, Quantification of acetylated IKK β normalized to total IKK β . Two-sided Mann–Whitney test. **c**, Determination of kinase activity. n = 2 independent experiments. **d, e**, BMDMs generated from *Apoe^{-/-}* mice were pretreated with varying concentrations of TMP195 or vehicle for 1 h and either stimulated with Tnf- α (50 ng/mL) or left untreated. **d**, Representative immunoblots of phosphorylated p65 at serine 536 and total p65 after 5 min of Tnf- α stimulation. **e**, Quantification of phosphorylated p65 normalized to total p65. n=8 independent experiments. One-way Anova with Holm-Sidak’s correction. **f**, Analysis of gene expression by RT-PCR after 24 h of Tnf- α stimulation. One-way Anova with Holm-Sidak’s correction. **g, h**, BMDMs generated from *Apoe^{-/-}* mice were treated with TMP195 (5 μM) or TPCA-1 (500 nM) for 1 h prior to stimulation with Tnf- α (50 ng/mL) for 24 h followed by RNA sequencing. **g**, Downregulated reactome pathways upon TMP195 treatment. **h**, Venn diagram depicting overlap between differentially regulated genes upon inhibition with TMP195 or TPCA-

1. TMP195 (n=5 mice) and TPCA-1 (n=5 mice). Results are log₂ fold change >1 or <-1 with *P*_{adj} ≤ 0.1. **i**, BMDMs generated from *ApoE*^{-/-} mice were treated with TMP195 (5 μM), TPCA-1 (500 nM), or co-treated with both inhibitors for 1 h prior to stimulation with Tnf-α for 24 h. Gene expression of key pro-inflammatory chemokines and cytokines was quantified by RT-PCR. One-way Anova with Fisher's LSD test. **P* < 0.05; ***P* < 0.01; ****P* < 0.001; *****P* < 0.001. Data are mean ± s.e.m.

Fig. 5. Therapeutic inhibition with TMP195 reduces atheroprogession and confers plaque stability. **a – d**, Experimental outline. *ApoE*^{-/-} mice receiving Western-type diet for 8 weeks were treated with TMP195 (50 mg/kg) or vehicle starting from the 5th week of diet, when lesions have already developed (**a**). **b**, Representative Oil-Red-O stained aortic root lesions. Scale bars, 200 μm. **c**, Quantification of lesion sizes. Two-sided Mann–Whitney test. **d**, Analysis of classical Ly6C^{hi} monocytes in atherosclerotic aortas. Two-sided unpaired t-test. **e – k**, Experimental outline. *ApoE*^{-/-} mice receiving Western-type diet for 11 weeks were treated with TMP195 (50 mg/kg) or vehicle starting from the 8th week of diet (**e**). **f**, Representative Sirius red stained lesions in the brachiocephalic artery. Scale bars, 100 μm. Quantification of lesion sizes (**g**), necrotic core area (**h**), fibrous cap (FC) thickness (**i**), smooth muscle cell area (**j**), and vulnerable plaque index (**k**). Two-sided unpaired t-test or Mann–Whitney test. **l**, Quantification of gene expression in atherosclerotic aortas. Two-sided Mann-Whitney test. **m – p**, Monocytes were freshly isolated from patients with established atherosclerosis and treated *ex vivo* with TMP195 or vehicle for 1 h prior to stimulation with TNF-α (50 ng/mL; **m**). **n**, Representative immunoblots of phosphorylated p65 at serine 536 and total p65 after 5 min of TNF-α stimulation. **o**, Quantification of phosphorylated p65 normalized to total p65 (n) and cytokine production after 24 h of TNF-α stimulation (**p**). One-way

Anova with Holm-Sidak's correction **o**). Two-sided unpaired t-test or Mann–Whitney test **p**). Data are mean \pm s.e.m.

Fig. 1

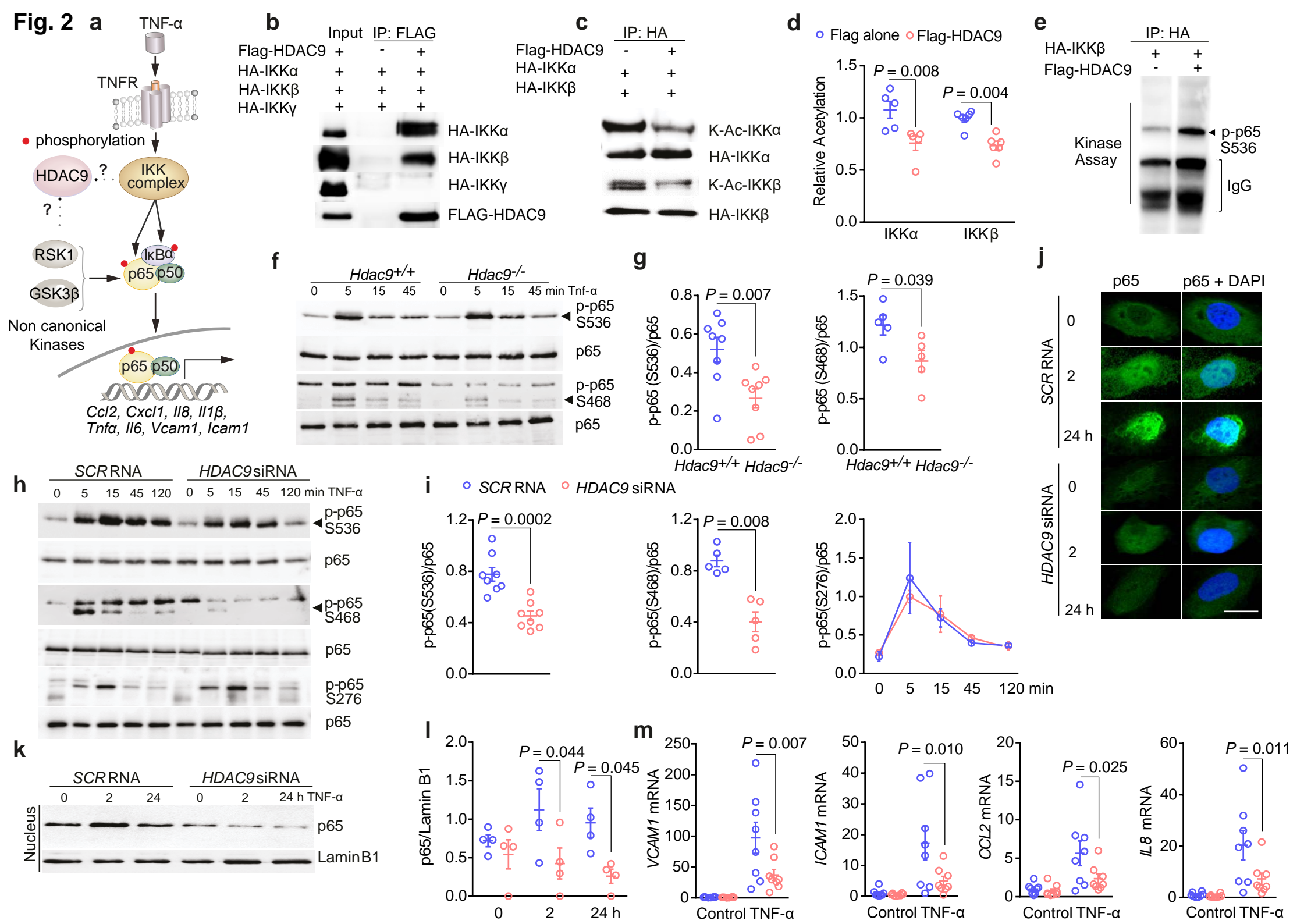


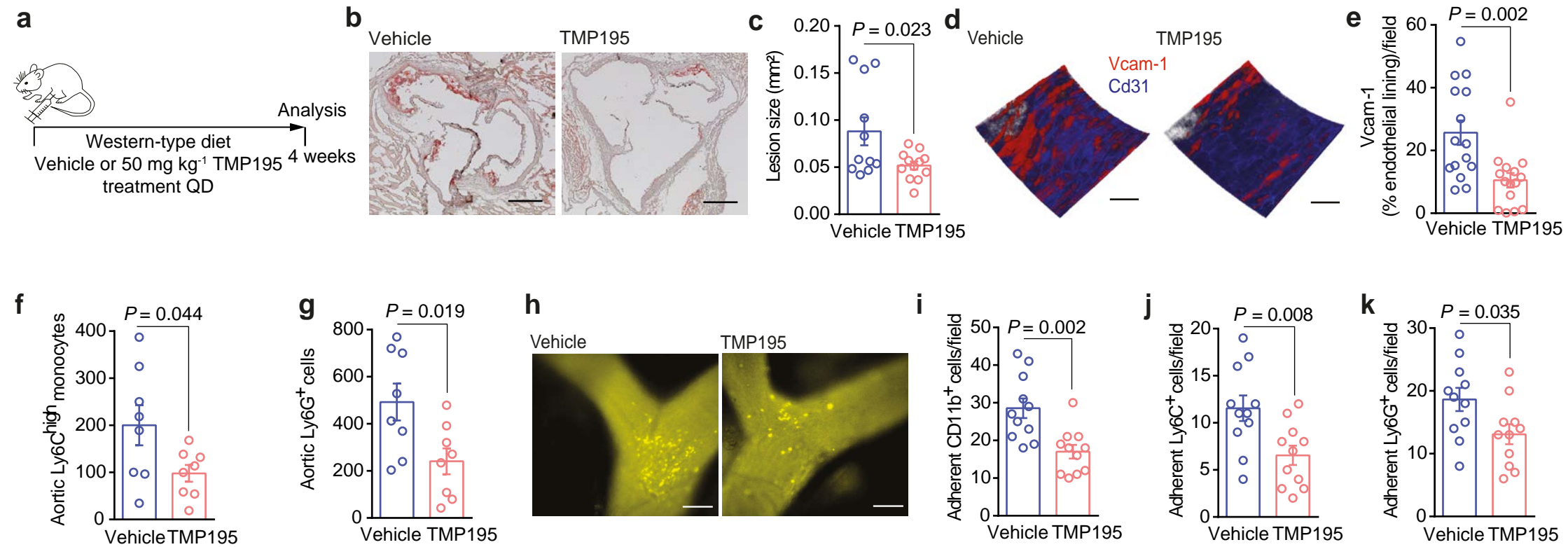
Fig. 3

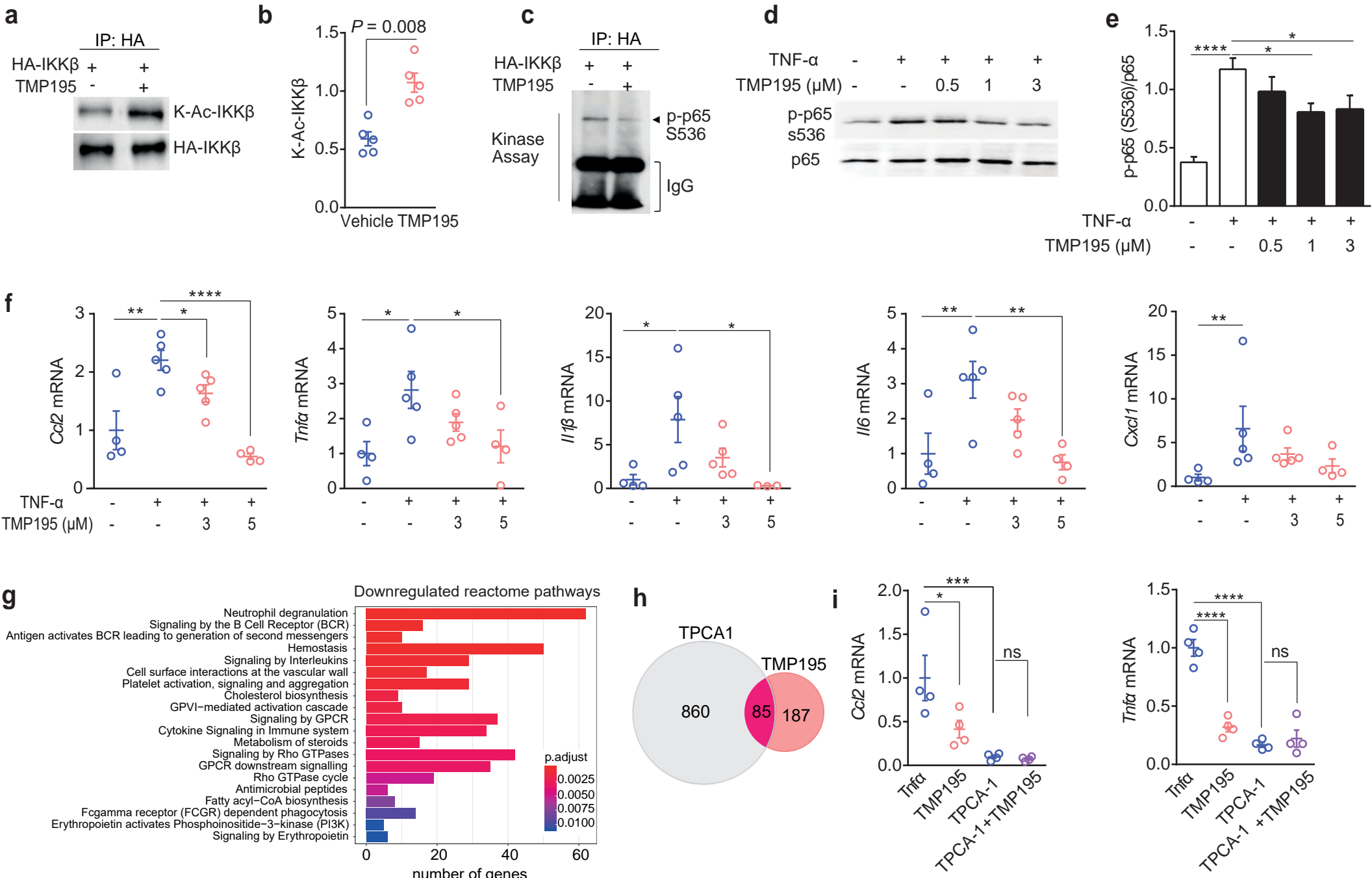
Fig. 4

Fig. 5